Bone Reports 14 (2021) 100745

Contents lists available at ScienceDirect

Bone Reports

journal homepage: www.elsevier.com/locate/bonr

Case Report

Imaging technologies in the differential diagnosis and follow-up of brown tumor in primary hyperparathyroidism: Case report and review of the literature

Davide Diacinti [a,b], Cristiana Cipriani [c,*], Federica Biamonte [a,c], Jessica Pepe [c], Luciano Colangelo [a,c], Endi Kripa [d], Antonio Iannacone [d], Martina Orlandi [d], Vito Guarnieri [e], Daniele Diacinti [d], Salvatore Minisola [c]

[a] Department of Oral and Maxillo-Facial Sciences, Sapienza University of Rome, Italy
[b] Department of Diagnostic and Molecular Imaging, Radiology and Radiotherapy, PTV Foundation "Tor Vergata" University, Rome, Italy
[c] Department of Clinical, Internal, Anesthesiological and Cardiovascular Sciences, Sapienza University of Rome, Italy
[d] Department of Radiological Sciences, Oncology and Anatomy-Pathology, Sapienza University of Rome, Italy
[e] Division of Medical Genetics, Fondazione IRCCS Casa Sollievo Della Sofferenza, San Giovanni Rotondo, Foggia, Italy

ARTICLE INFO

Keywords:
Brown tumor
Primary hyperparathyroidism
Parathyroid adenoma
MRI

ABSTRACT

Brown tumors are osteolytic lesions associated with hyperparathyroidism (HPT). They may involve various skeletal segments, but rarely the cranio-facial bones. We report a case of a young boy with a swelling of the jaw secondary to a brown tumor presenting as the first manifestation of primary HPT (PHPT). He was found to have brown tumor located in the skull, as well. Different imaging technologies were employed for the diagnosis and follow-up after parathyroidectomy. We enclose a review of the literature on the employment of such imaging technologies in the differential diagnosis of osteolytic lesions. A multidisciplinary approach comprising clinical, laboratory and imaging findings is essential for the differential diagnosis of brown tumor in PHPT.

1. Introduction

Brown tumors are osteolytic giant-cell lesions originating from the increased osteoclasts activity in the setting of chronically elevated parathyroid function as both primary and secondary hyperparathyroidism (HPT) (Triantafillidou et al., 2006). Brown tumors involve more frequently the ribs, clavicle, tibia, femur, pelvic girdle and hands (Elqatni et al., 2011), while rarely the maxillo-facial bones (4.5% of cases) (Slama et al., 2007; Lessa et al., 2005; Keyser and Postma, 1996). It is not easy to distinguish them from osteolytic metastases or lesions from multiple myeloma, with which they share similar characteristics (Kalathas et al., 2010). Diagnosis is even more difficult in cases of Brown tumors at unusual localization.

We report a case of brown tumor of the jaw as the first clinical presentation in a young patient with primary hyperparathyroidism (PHPT) including description of the differential diagnosis of the lesion and the follow-up after surgery by X-ray and magnetic resonance imaging (MRI). We also included a review of the literature on the radiological workup in the differential diagnosis of brown tumor in PHPT patients.

2. Case description

2.1. Clinical presentation and laboratory assessment

A 19-year old boy was admitted to the Dental Clinic with painful swelling of the oral cavity involving the mandible. An orthopantomography showed a large osteolytic lesion in left inferior alveolar arch between the third and fourth quadrants involving the cortical bone of the mandible. A Computed Tomography exam confirmed a large and multiloculated osteolytic lesion on the left mandible with cranial extension to the half anterior portion of the jaw. Biochemical tests were performed showing elevated serum calcium levels, both the total (16.1 mg/dl; normal range: 8.2 to 10.2 mg/dl) and ionized calcium (2.13 mmol/l;

* Corresponding author.
E-mail addresses: davide.diacinti@uniroma1.it (D. Diacinti), cristiana.cipriani@gmail.com (C. Cipriani), jessica.pepe@uniroma1.it (J. Pepe), luciano.colangelo@uniroma1.it (L. Colangelo), endi.kripa@uniroma1.it (E. Kripa), v.guarnieri@operapadrepio.it (V. Guarnieri), daniele.diacinti@uniroma1.it (D. Diacinti), salvatore.minisola@uniroma1.it (S. Minisola).

https://doi.org/10.1016/j.bonr.2020.100745
Received 22 September 2020; Received in revised form 5 December 2020; Accepted 28 December 2020
Available online 30 December 2020

normal range: 1.17–1.33 mmol/l); serum PTH levels were very high (1028 pg/ml; normal range: 15–65 pg/ml); serum phosphate and 25-hydrohy-vitamin D [25(OH)D] levels were reduced (2.2 mg/dl; normal range: 2.5–4.6 mg/dl and 8 ng/ml; insufficiency < 20 ng/ml); serum alkaline phosphatase was elevated (442 U/l; normal range: 40–129).

2.2. Imaging of the parathyroid glands

Neck ultrasound and scintigraphy with dual tracer technetium-99 m (99-mTc)-pertecnetato 207 MBq + 99mTc-MIBI 408 MBq sestamibi and subtraction after 2 h detected an abnormal parathyroid gland. Neck ultrasound images are illustrated in Fig. 1a. It shows a solid, hypoechoic, oblong, well-circumscribed mass with signal color-Doppler of monopolar vascular pattern referred to "as the arc or rim sign", located posterior-inferiorly to the left thyroid lobe; these ultrasound features were typical of the parathyroid adenoma. The 99-mTc sestamibi scintigraphy showed a residual uptake caudally to the left thyroid lobe (Fig. 1c).

2.3. Imaging of the brown tumors

The MRI of the mandible and the neck region was performed to more accurately localize and characterize both the enlarged parathyroid gland and the mandibular lesion. We employed the parathyroid-dedicated protocol for obtaining the neck images (Sacconi et al., 2016) and observed an elongated mass of 16 × 12 × 26 mm posterior-inferiorly to the left thyroid lobe, with hyper-intensity on the T2-weighted IDEAL FSE images, rapid and strong enhancement in comparison to the normal thyroid tissue on T1 post-contrast sequences and cleavage plane with the thyroid gland (Fig. 1b–e). According to the diagnostic MRI criteria described in our previous study (Sacconi et al., 2016; Argiro et al., 2018), the mass was diagnosed as parathyroid adenoma.

As far as the left mandible MRI images, the T1-weighted post-contrast images showed an enhanced solid multi-loculated and lytic formation of 43 × 28 mm diameter involving the cancellous bone with thinning of cortical bone, suspicious for jaw brown tumor (Fig. 1e). Total skeletal conventional X-rays exam was then performed and confirmed the multi-loculated lytic mass of the left mandible. Additionally, another lytic lesion was visualized in the right parietal bone of the skull. Both osteolytic lesions were interpreted as possible brown tumors in the setting of PHPT (Fig. 1d). Hand X-rays showed sub-periosteal bone resorption.

Total body bone scintigraphy (99mTc-HDP 791 MBq) revealed an uptake of the jaw and of the right parietal bone confirming the radiological findings (Fig. 1f).

2.4. Other diagnostic tests

Dual X-ray absorptiometry (DXA) was performed at the lumbar spine (L1-L4: BMD 0.900 g/cm^2; Z score −1.6), femoral neck (BMD 0.777 g/cm^2; Z score −1.1), total femur (BMD 0.856 g/cm^2; Z score: −1.2) and

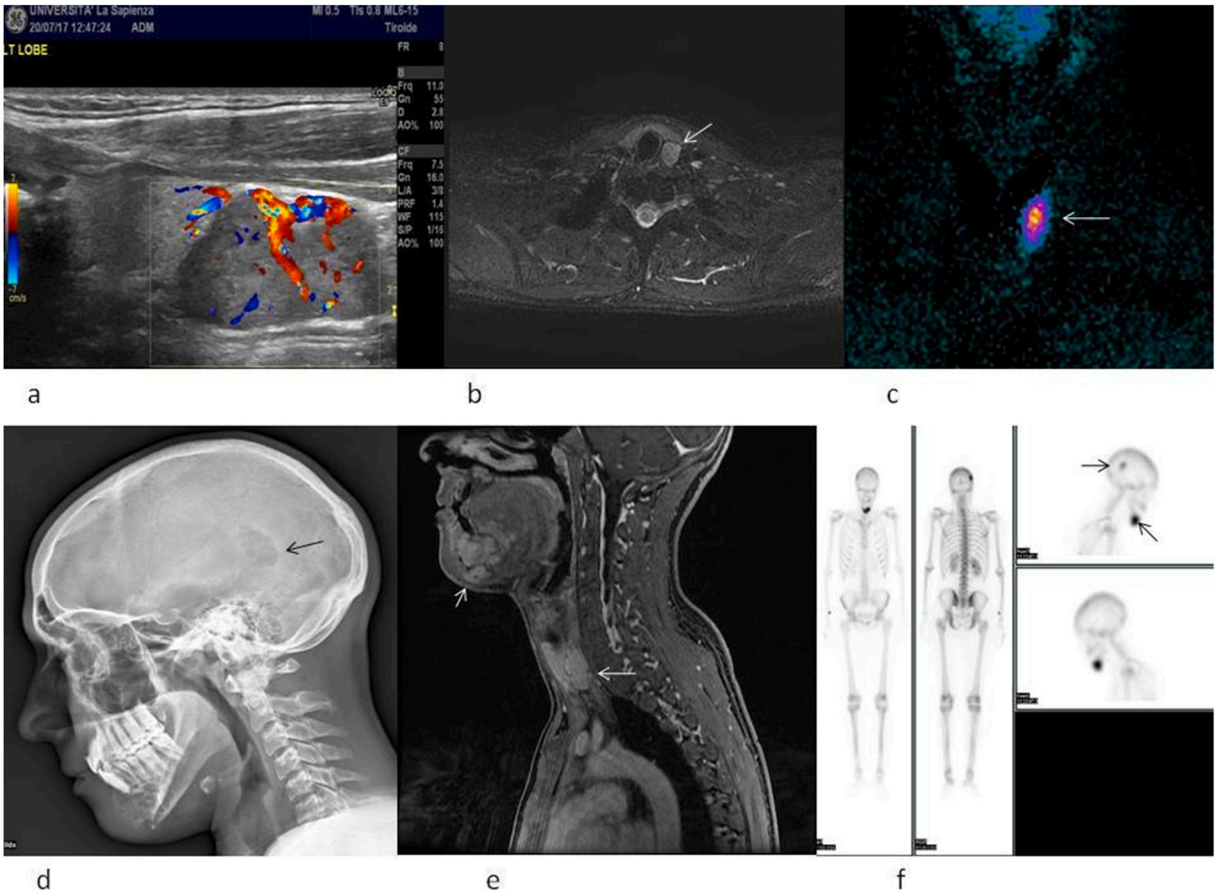

Fig. 1. a) Ultrasound image showing the parathyroid adenoma as an oblong hypo-echoic and capsulated lesion with signal color-Doppler of monopolar vascular pattern referred to as the arc or rim sign, posterior-inferiorly to the left thyroid lobe; b) Axial T2 IDEAL Fat Suppressed MRI image depicting hyperintense parathyroid adenoma posterior-inferiorly to the left thyroid lobe, and separated from the thyroid gland (arrow); c) 99-mTc sestamibi scan demonstrating a residual uptake on left side 2 h after the radiotracer administration (arrow); d) X-ray image of the skull showing an osteolytic lesion with lobulated margin in the right parietal bone (arrow); e) Sagittal post-contrast T1-weighted MRI image showing enhancement of the parathyroid adenoma and of the jaw brown tumor (arrow); f) 99-mTc scan demonstrating uptake of the jaw bone and of the right parietal lobe of the skull (arrow).

distal 1/3 radius (BMD: 0.563 g/cm^2; Z score: −4.6).

Given the young age and the diagnosis of PHPT in association with the lesion of the mandible, the diagnosis of hyperparathyroidism-jaw tumor syndrome (HPT-JT) was first considered and genetic tests were performed. The CDC73 gene was sequenced and no mutation was found.

2.5. Surgery

Patient underwent removal of the left inferior parathyroid gland and left thyroid lobe excision. Intraoperative PTH levels decreased from 886 pg/ml at baseline to 80 pg/ml at 15 min. The parathyroid lesion was 32 × 16 × 15 mm diameter (Fig. 2a). Histopathological examination confirmed the diagnosis of parathyroid adenoma. The adenoma weighted 3 g.

Patient was discharged 7 days after surgery. Laboratory exams at discharge were: serum calcium 8.8 mg/dl; serum PTH 80 pg/ml; serum 25(OH)D 9 ng/ml. Supplementation with calcium carbonate (1000 mg twice a day) and oral cholecalciferol (weekly 50,000 IU for 4 weeks followed by monthly 50,000 IU) was started.

2.6. Follow-up

Six months after parathyroidectomy, biochemical parameters were:

Serum calcium: 9.1 mg/dl; PTH 30 pg/ml; phosphate 2.3 mg/dl; 25 (OH)D 35 ng/ml; alkaline phosphatase 140 U/l. Follow-up MRI showed a reduction of the brown tumors localized in the left mandible with diameter of about 35 × 24 mm; reduction of signal intensity in T2-weighted sequences compared to the pre-surgery exam was evident together with T1 images minimal post-contrast enhancement that persisted only in some peripheral areas (Fig. 2b–c). These MRI findings were ascribed to the partial regression of the brown tumors following parathyroidectomy.

Skull X-rays exam showed the complete sclerosis of the lesion in the right parietal bone and partial sclerosis of the lesion in the left mandible (Fig. 2d).

3. Discussion and review of the literature

We described a rare clinical presentation of PHPT in a young patient

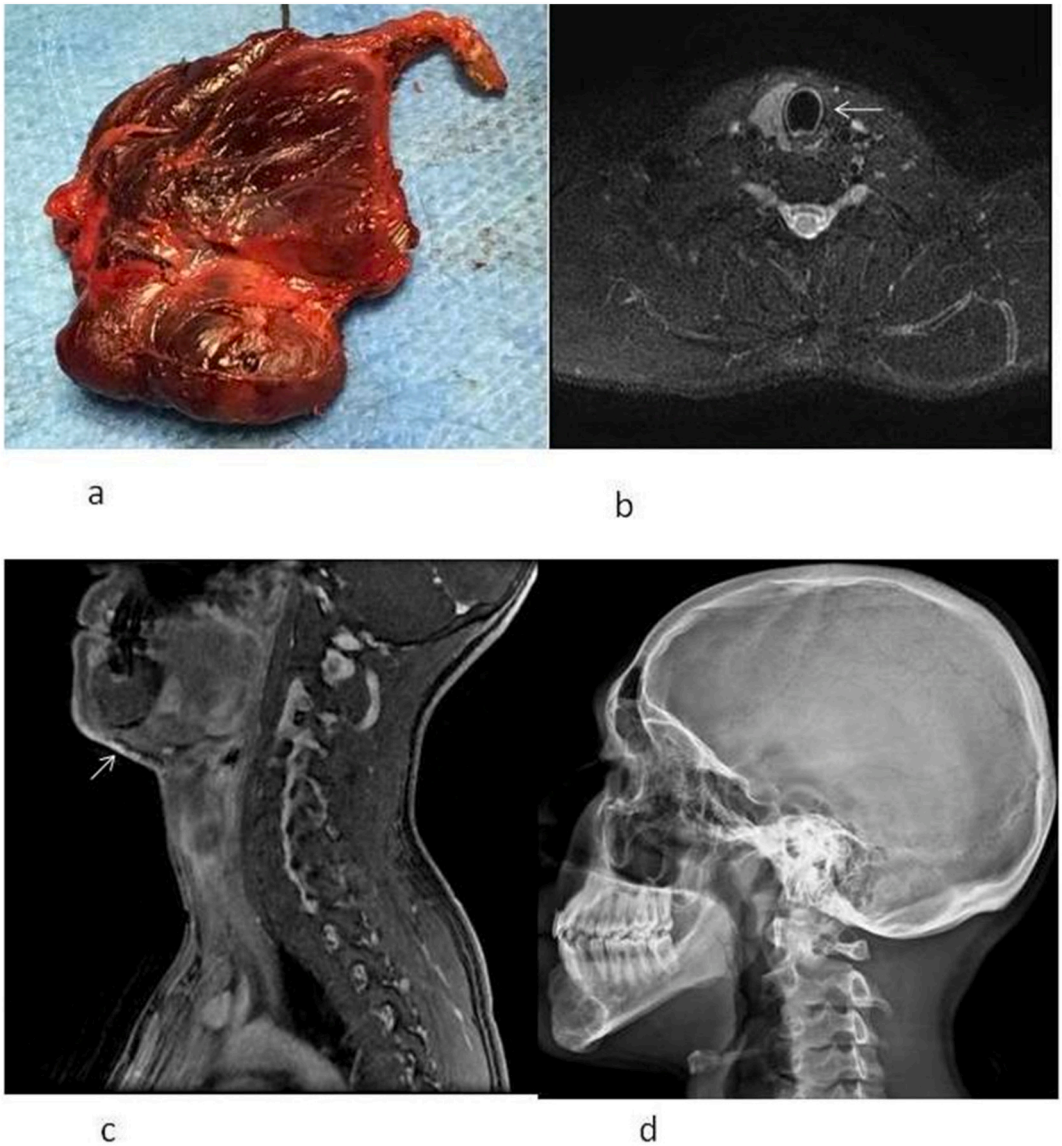

Fig. 2. Six-month post-surgery images. a) Parathyroid adenoma; b) Axial T2 IDEAL Fat Suppressed MRI image showing surgical resection of the parathyroid adenoma and of the left thyroid lobe (arrow); c) Sagittal post-contrast T1-weighted MRI showing almost absent contrast enhancement of the brown tumor, excluding persistence of contrast peripheral enhancement in some areas of the lesion (arrow); d) X-ray image of the skull showing no evidence of the previous osteolytic lesion in the right parietal bone.

in which the integration of clinical history, laboratory findings and the use of different imaging technologies were essential for the final diagnosis and follow-up. Brown tumors, particularly located in the maxilla-facial bones, are currently uncommon complications of PHPT and have been rarely described as first clinical presentation of the disease (Lessa et al., 2005; Cipriani and Bilezikian, 2019).

Clinical presentation of PHPT is classified according to the three well-known phenotypes of symptomatic, asymptomatic and normocalcemic PHPT (Cipriani and Bilezikian, 2019). Symptomatic PHPT is characterized by overt classical complications involving the skeleton and the kidneys, such as bone erosions, subperiosteal bone resorption of the fingers, brown tumors, "salt and pepper" appearance of the skull, nephrolithiasis and nephrocalcinosis (Bilezikian et al., 2018). Asymptomatic PHPT is diagnosed by determination of serum calcium during routine biochemical screening, and most commonly seen in the Western countries. Finally, normocalcemic PHPT is diagnosed when serum total and ionized calcium levels are normal, serum PTH is elevated and secondary causes of HPT have been excluded (Cipriani and Bilezikian, 2019).

With reference to skeletal complications, brown tumors are observed in 4.5% of patients with PHPT and 1.5–1.7% of those with secondary HPT in the setting of chronic kidney disease, mostly in women older than 50 (Lessa et al., 2005; Keyser and Postma, 1996; Brabyn et al., 2017). There have been few reports of brown tumors in patients with normocalcemic PHPT (Cebesoy et al., 2007). Brabyn et al. reported that the mandible was the most common localization for the maxilla-facial brown tumors associated with PHPT (Brabyn et al., 2017). These tumors are usually slow-growing, palpable, swelling lesions, sometimes locally aggressive and causing facial deformity or pathologic fractures (Palla et al., 2018). However they can be asymptomatic in some cases (Takeshita et al., 2006). A small number of patients with PHPT and maxillo-facial bone lesions present a rare hereditary syndrome known as hyperparathyroioidism-jaw tumor syndrome (HPT-JT). It is an autosomal dominant genetic syndrome characterized by mutation of the HRTP2 gene encoding the parafibromin (Carpten et al., n.d.). In addition to PHPT, patients present with ossifying fibromas of the mandible and maxilla that do not regress after parathyroid surgery; renal tumors or uterine fibroids may be associated (Simonds et al., 2002). Given his young age and the bone lesion of the jaw as first clinical presentation, the genetic workup was first performed for excluding the HPT-JT syndrome in our patient. Nevertheless, the radiological characteristics of the lesion of the jaw and the finding of the skull lesion, in association with the laboratory exams, finally oriented towards the diagnosis of brown tumors in the setting of PHPT.

The histopathology of brown tumors resembles that of the fibrous dysplasia (FD) and giant cells tumors (GCT) because of their dense fibroblastic stroma and the presence of many macrophages, multinucleated giant osteoclastic cells, and hemosiderin deposits consequent to focal hemorrhage. The color of these deposits determined the name "brown tumor" (Rosenberg, 2001).

From the radiological point of view, brown tumors appear as well defined, lucent, lytic lesion on X-ray, with thin or broken cortex, but no specific signs (Rossi et al., 2014). Signs of PHPT, as subperiosteal bone resorption, disappearance of the lamina dura around the roots of the teeth and generalized osteopenia maybe associated (Elqatni et al., 2011; Takeshita et al., 2006). Computed Tomography (CT) images of brown tumor show irregular, multi-loculated osteolytic lesions, with "ground glass opacification" involving the cortex that may be interrupted; contrary to bone cysts, these lesions take the contrast media (Takeshita et al., 2006). By MRI, brown tumors are visualized as three possible types of lesion, according to Hong et al. (Hong et al., 2011) (Table 1). They are: solid lesions with iso- hypo-intense signal on T1- and T2-weighted images and contrast enhancement after intravenous gadolinium; mixed solid and cystic lesions with T1-weighted hypo-intense signal and T2-weighted iso- or hypo-intense signal, contrast enhancement of the solid portions and the septa of cystic lesions; cystic lesions with T2-weighted hyper-intensity and contrast enhancement from the periphery and septa of the cyst. Brown tumors may have recurrent intralesion bleeding that is seen as a fluid-fluid level by MRI (Takeshita et al., 2006). The association of a shortened T2 time-relaxation by MRI due to the presence of hemosiderin deposition with an osteolytic lesion visualized by standard X-ray would be the most specific criterion for diagnosis of brown tumor (Miyakoshi et al., 2007).

The differential diagnosis of brown tumor may be challenging. They

Table 1
Main characteristics of osteolytic lesions as visualized by X-ray, CT, MRI and bone scintigraphy and biochemical abnormalities.

	Brown tumor	Fibrous dysplasia	Giant cell tumor	Aneurysmal bone cyst	Lytic metastasis	Multiple myeloma
X-ray	Well defined lytic lesions, radiolucent; thin or broken cortex; X-ray signs of PHPT	Focal lytic, mixed or sclerotic lesion	Solid or mixed well defined solid-cystic lesion; bone expansion; cortical thinning; non-sclerotic margins	Focal, multi lobulated, pseudocyst; lytic lesions; thin sclerotic margins	Focal, lytic lesions; bone destruction; narrow zones of transition; periosteal reaction	Lytic expansive lesions; prominent cortical thinning; well defined, non-sclerotic margins
CT	Irregular, multi-loculated lytic lesions; "ground glass opacification" and interruption of the cortex; contrast enhancement	Ground-glass matrix; mixed pattern of ground glass, lytic or sclerotic appearance	Solid or mixed solid-cystic lesion; bone expansion; hyper-dense solid components with contrast enhancement	Focal, multi-lobulated, pseudocyst; lytic lesions with fluid-fluid levels; cortical thinning; no contrast enhancement	Lytic lesions; poorly defined margins; bone destruction	Punched-out expansive lytic lesions
MRI	isohypo-intense signal in T1, T2-weighted sequences; contrast enhancement of the solid portions and septa of cystic lesions; T2 hyper-intense in cystic lesion and contrast enhancement from the periphery and septa	Low signal intensity on T1-T2-weighted images in ossified or fibrous portions; heterogeneous enhancement and signal intensity in the active phase.	Hypo-isointense signal on T1-weighted sequence; hypo-intensity on T2; heterogeneous contrast enhancement	Different T1 and T2 intensity signal of intra-cavitary fluid-fluid levels; surrounding rim of low T1 and T2 signal; possible septa enhancement	Soft hypo-intense tissue on T1 replacing bone marrow; heterogeneous contrast enhancement	Hypo-isointense signal on T1; hyper-intense signal on T2-fat suppression sequences; early contrast enhancement
Bone scintigraphy	Increased focal uptake	Increased focal uptake	Increased periferic uptake with central photopenia ("donut sign")	Homogeneous increased or mild uptake	Increased focal or diffuse uptake	Increased uptake
Total calcium	High	Normal	Normal	Normal	High	High/normal
PTH	High	High/Normal	Normal	Normal	Low	Low/normal
Alkaline Phosphatase	High	High/Normal	Normal	Normal	High	Normal

can mimic other lesions, such as FD, GCT, aneurysmal bone cyst, cancer, metastases, and multiple myeloma (Lessa et al., 2005). Hence, clinical history, localization of the lesions, laboratory exams, and the employment of different imaging technologies (X-ray, MRI, CT) exploring several areas (e.g. the cortex, bone marrow, soft tissue surrounding the lesion, etc.) and aspects (e.g. presence of hemorrhage or hemosiderin deposits, sclerosis, multi-loculated lesion, etc.) of the lesion are essential during the diagnostic workup. Table 1 summarizes the most relevant aspects of these lesions as visualized by X-ray, CT and MRI and their main characteristics on bone scintigraphy.

FD lesions may involve long bones, craniofacial bones or the ribs; they are visualized as focal lytic, mixed or sclerotic, radiolucent and well-defined lesions in the early stage, mottled and radio-opaque during disease progression on X-ray (Chapurlat and Orcel, 2008). CT evidence of "ground-glass" matrix of the woven bone associated with lytic or sclerotic lesions is useful for diagnosis (Hocaoglu et al., 2014). MRI examination shows low signal intensity images on T1 and T2 in the ossified or fibrous portions, heterogeneous enhancement and signal intensity in the active phase, intra-lesion cellularity, and hemorrhagic or cystic components (Lisle et al., 2008).

Similarly to brown tumors, GCT are frequently (33%–57% of cases) multi-loculated lytic lesions, with cortical thinning, narrow zone of transition but no sclerotic margins on X-ray (Hudson et al., 1984). CT is useful in better defining cortical thinning, pathologic fracture, periosteal reaction, degree of osseous expansive remodeling and the solid components that show contrast enhancement (Manaster and Doyle, 1993). By MRI, GCT shows hypo- isointense signal in T1 and hypo-intense signal in T2-weighted sequences due to hemosiderin deposition or increased cellularity, high collagen content, and heterogeneous contrast enhancement (Murphey et al., 2001).

Aneurysmal bone cysts are benign intra-osseous lesions that, similarly to brown tumors, are rarely (2% of cases) located in the craniofacial skeleton and mostly in the metaphyses of long bones (Kalantar Motamedi, 1998). The integrated use of different imaging technologies is usually needed for the differential diagnosis (Motamedi et al., 2008). X-ray shows a focal multi-lobulated, pseudocyst, lytic lesion with thin sclerotic margins (Motamedi et al., 2008); CT demonstrates bone expansion and cortical thinning (Motamedi et al., 2008); MRI shows intra-cavitary fluid-fluid levels due to the blood degradation products and possible septations enhancement (Motamedi et al., 2008).

The diagnosis of lytic metastases should be considered in case of X-ray and CT images of focal lytic lesions with poorly defined margins, bone destruction, narrow zones of transition, and periosteal reaction; the associated soft tissue has different density and heterogeneous contrast enhancement on CT (Mulligan and Murphey, 2008). Soft tissue is visualized as hypo-intense on T1-weighted MRI images and replaces the normal hyper-intense signal of bone marrow and has heterogeneous contrast enhancement (Kee et al., 2020).

The typical imaging pattern of multiple myeloma is characterized by punched out lytic lesions, prominent cortical thinning and well defined but non-sclerotic margins on X-ray and CT (Zamagni and Cavo, 2019). MRI is useful for diagnosis as it shows hypo-isointense signal on T1-weighted sequences; hyper-intense signal in T2- fat suppression sequences and early contrast enhancement (Hanrahan et al., 2010).

As far as other technologies, bone scintigraphy is sensitive but not specific for the diagnosis of many skeletal lesions (Rybak and Rosenthal, 2001). Brown tumors, as well as the other aforementioned disorders, show increased focal or diffuse radionuclide uptake; only GCT present increased peripheral uptake with central areas of photopenia ("donut sign") (Levine et al., 1984). In all cases, bone scintigraphy is particularly useful in detecting multifocal bone involvement (Elqatni et al., 2011; Kalathas et al., 2010; van Baardwijk et al., 2006).

Imaging technologies were successfully employed during follow-up after parathyroid surgery in our patient. The lack of a total size reduction of the left mandible brown tumor could be ascribed to the short follow-up time (6 months), as other factors that reduce the likelihood of regression were not present in our patient. Historical reports indeed observed that the extensive bone involvement with consequent destructive effects, and older age are the main factors associated with lower rate of regression of brown tumors after parathyroidectomy (Kar et al., 2001; Daniels, 2004).

The study of skeletal complications of PHPT was completed in our patient by the assessment of BMD that did not show very low values at the lumbar spine and hip as could be predicted from very high PTH and alkaline phosphatase levels, as well as the presence of brown tumor. Reasons for such a discrepancy could be many. First, the brown tumor of the mandible was the onset manifestation of the disease, and no laboratory workup including assessment of parameters of mineral metabolism had been performed before this clinical manifestation. Hence, we could hypothesize that disease duration was not as long as to determine significant reduction of the BMD at least at the lumbar spine and hip. Indeed, we observed a very low BMD value at the cortical site (1/3 radius), where the high PTH levels exerts its major detrimental effect. Additionally, notwithstanding high serum PTH and alkaline phosphatase levels are usually associated with very low BMD in PHPT patients on average, this could be not seen in any given case. Finally, young patient's age may be another factor to consider in this scenario.

In conclusion, our case report demonstrates that a multi-disciplinary clinical, laboratory and radiological approach is mandatory for the differential diagnosis of osteolytic lesions, particularly when manifesting with unusual clinical presentation. X-ray, CT and MRI should be used as integrated imaging technologies during the diagnostic workup and the follow-up. The knowledge of the main radiological characteristics of skeletal disease associated with osteolytic lesions is useful in patient's clinical assessment.

Consent to participate

Written informed consent and permissions were obtained from patient.

Authors' contributions

DD, CC and SM contributed to data collection, drafting and revision of the manuscript.

FB, JP, LC, EK, AI, MO, VC, DD contributed to patient's management and data collection.

All authors have approved the final version of the manuscript.

Funding

None.

Declaration of competing interest

S.M. served as speaker for Abiogen, Amgen, Bruno Farmaceutici, Diasorin, Eli Lilly, Shire, Sandoz, Takeda. He served in advisory board of Abiogen, Kyowa Kirin, Pfizer, UCB. All other authors declare no conflict of interests.

References

Argiro, R., Diacinti, D., Sacconi, B., Iannarelli, A., Diacinti, D., Cipriani, C., Pisani, D., Romagnoli, E., Biffoni, M., Di Gioia, C., Pepe, J., Bezzi, M., Letizia, C., Minisola, S., Catalano, C., 2018. Diagnostic accuracy of 3T magnetic resonance imaging in the preoperative localisation of parathyroid adenomas: comparison with ultrasound and 99mTc-sestamibi scans. Eur. Radiol. 28, 4900–4908.

Bilezikian, J.P., Bandeira, L., Khan, A., Cusano, N.E., 2018. Hyperparathyroidism. Lancet 391, 168–178.

Brabyn, P., Capote, A., Belloti, M., Zylberberg, I., 2017. Hyperparathyroidism diagnosed due to Brown tumors of the jaw: a case report and literature review. Journal of oral and maxillofacial surgery : official journal of the American Association of Oral and Maxillofacial Surgeons 75, 2162–2169.

Carpten JD, Robbins CM, Villablanca A, Forsberg L, Presciuttini S, Bailey-Wilson J, Simonds WF, Gillanders EM, Kennedy AM, Chen JD, Agarwal SK, Sood R, Jones MP,

Moses TY, Haven C, Petillo D, Leotlela PD, Harding B, Cameron D, Pannett AA, Hoog A, Heath H, 3rd, James-Newton LA, Robinson B, Zarbo RJ, Cavaco BM, Wassif W, Perrier ND, Rosen IB, Kristoffersson U, Turnpenny PD, Farnebo LO, Besser GM, Jackson CE, Morreau H, Trent JM, Thakker RV, Marx SJ, Teh BT, Larsson C, Hobbs MR (2002) HRPT2, encoding parafibromin, is mutated in hyperparathyroidism-jaw tumor syndrome. Nature genetics 32:676–680.

Cebesoy, O., Karakok, M., Arpacioglu, O., Baltaci, E.T., 2007. Brown tumor with atypical localization in a normocalcemic patient. Arch. Orthop. Trauma Surg. 127, 577–580.

Chapurlat, R.D., Orcel, P., 2008. Fibrous dysplasia of bone and McCune-Albright syndrome. Best Pract. Res. Clin. Rheumatol. 22, 55–69.

Cipriani, C., Bilezikian, J.P., 2019. Three generational phenotypes of sporadic primary hyperparathyroidism: evolution defined by technology. The lancet. Diabetes & endocrinology 7, 745–747.

Daniels, J.S., 2004. Primary hyperparathyroidism presenting as a palatal brown tumor. Oral surgery, oral medicine, oral pathology, oral radiology, and endodontics 98, 409–413.

Elqatni, M.F.J., Hammi, S., Jira, M., Elomri, N., Sekkach, Y., et al., 2011. Une tuméfaction digitale. Rev Med Interne 32, 48–49.

Hanrahan, C.J., Christensen, C.R., Crim, J.R., 2010. Current concepts in the evaluation of multiple myeloma with MR imaging and FDG PET/CT. Radiographics : a review publication of the Radiological Society of North America, Inc 30, 127–142.

Hocaoglu, E., Yirgin, I.K., Aksoy, S., Arslan, G., Inci, E., Cimilli, T., 2014. Computed tomography imaging findings of craniofacial fibrous dysplasia. The Journal of craniofacial surgery 25, 1175–1177.

Hong, W.S., Sung, M.S., Chun, K.A., Kim, J.Y., Park, S.W., Lee, K.H., Lim, H.W., Lim, Y.S., Yoo, W.J., Chung, M.H., 2011. Emphasis on the MR imaging findings of brown tumor: a report of five cases. Skelet. Radiol. 40, 205–213.

Hudson, T.M., Schiebler, M., Springfield, D.S., Enneking, W.F., Hawkins Jr., I.F., Spanier, S.S., 1984. Radiology of giant cell tumors of bone: computed tomography, arthro-tomography, and scintigraphy. Skelet. Radiol. 11, 85–95.

Kalantar Motamedi, M.H., 1998. Aneurysmal bone cysts of the jaws: clinicopathological features, radiographic evaluation and treatment analysis of 17 cases. Journal of cranio-maxillo-facial surgery : official publication of the European Association for Cranio-Maxillo-Facial Surgery 26, 56–62.

Kalathas, T., Kalatha, T., Boultoukas, E., 2010. Brown tumors; a possible pitfall in diagnosing metastatic disease. Hellenic journal of nuclear medicine 13, 15–17.

Kar, D.K., Gupta, S.K., Agarwal, A., Mishra, S.K., 2001. Brown tumor of the palate and mandible in association with primary hyperparathyroidism. Journal of oral and maxillofacial surgery : official journal of the American Association of Oral and Maxillofacial Surgeons 59, 1352–1354.

Kee, T.P., Liauw, L., Sathiyamoorthy, S., Lee, H.Y., Tan, G.S.L., Yu, W.Y., 2020. Large solitary lytic skull vault lesions in adults: radiological review with pathological correlation. Clin. Imaging 59, 129–143.

Keyser, J.S., Postma, G.N., 1996. Brown tumor of the mandible. Am. J. Otolaryngol. 17, 407–410.

Lessa, M.M., Sakae, F.A., Tsuji, R.K., Filho, B.C., Voegels, R.L., Butugan, O., 2005. Brown tumor of the facial bones: case report and literature review. Ear, nose, & throat journal 84, 432–434.

Levine, E., De Smet, A.A., Neff, J.R., Martin, N.L., 1984. Scintigraphic evaluation of giant cell tumor of bone. AJR Am. J. Roentgenol. 143, 343–348.

Lisle, D.A., Monsour, P.A., Maskiell, C.D., 2008. Imaging of craniofacial fibrous dysplasia. Journal of medical imaging and radiation oncology 52, 325–332.

Manaster, B.J., Doyle, A.J., 1993. Giant cell tumors of bone. Radiol. Clin. N. Am. 31, 299–323.

Miyakoshi, M., Kamoi, K., Takano, T., Nishihara, M., Kawashima, T., Sudo, N., Togashi, K., Emura, I., Williams, D., 2007. Multiple brown tumors in primary hyperparathyroidism caused by an adenoma mimicking metastatic bone disease with false positive results on computed tomography and Tc-99m sestamibi imaging: MR findings. Endocr. J. 54, 205–210.

Motamedi, M.H., Navi, F., Eshkevari, P.S., Jafari, S.M., Shams, M.G., Taheri, M., Abbas, F.M., Motahhari, P., 2008. Variable presentations of aneurysmal bone cysts of the jaws: 51 cases treated during a 30-year period. Journal of oral and maxillofacial surgery : official journal of the American Association of Oral and Maxillofacial Surgeons 66, 2098–2103.

Mulligan, M.E.F.D., Murphey, M.D., 2008. Metastatic disease. In: Musculoskeletal imaging, 2nd edition. Elsevier, Philadelphia, PA, pp. 1016–1032.

Murphey, M.D., Nomikos, G.C., Flemming, D.J., Gannon, F.H., Temple, H.T., Kransdorf, M.J., 2001. From the archives of AFIP. Imaging of giant cell tumor and giant cell reparative granuloma of bone: radiologic-pathologic correlation. Radiographics : a review publication of the Radiological Society of North America, Inc 21, 1283–1309.

Palla, B.B.E., Fliefel, R., Otto, S., 2018. Systematic review of oral manifestations related to hyperparathyroidism. Clin. Oral Investig. 22, 1–27.

Rosenberg, A.E.N.G., 2001. Giant cell containing lesions of bone and their differential diagnosis. Curr. Diagn. Pathol. 7, 235–246.

Rossi, B.F.V., Appetecchia, M.L., Novello, M., Zoccali, C., 2014. Giant cell tumor of bone in a patient with diagnosis of primary hyperparathyroidism: a challenge in differential diagnosis with brown tumor. Skelet. Radiol. 43, 693–697.

Rybak, L.D., Rosenthal, D.I., 2001. Radiological imaging for the diagnosis of bone metastases. The quarterly journal of nuclear medicine : official publication of the Italian Association of Nuclear Medicine 45, 53–64.

Sacconi, B., Argiro, R., Diacinti, D., Iannarelli, A., Bezzi, M., Cipriani, C., Pisani, D., Cipolla, V., De Felice, C., Minisola, S., Catalano, C., 2016. MR appearance of parathyroid adenomas at 3 T in patients with primary hyperparathyroidism: what radiologists need to know for pre-operative localization. Eur. Radiol. 26, 664–673.

Simonds, W.F., James-Newton, L.A., Agarwal, S.K., Yang, B., Skarulis, M.C., Hendy, G.N., Marx, S.J., 2002. Familial isolated hyperparathyroidism: clinical and genetic characteristics of 36 kindreds. Medicine 81, 1–26.

Slama, A.M.Z., Walha, L., Sriha, B., Kochtali, H., 2007. Le stumeurs brunes maxillaires. Actualités Odonto Stomatologiques 169–176.

Takeshita, T., Takeshita, K., Abe, S., Takami, H., Imamura, T., Furui, S., 2006. Brown tumor with fluid-fluid levels in a patient with primary hyperparathyroidism: radiological findings. Radiat. Med. 24, 631–634.

Triantafillidou, K., Zouloumis, L., Karakinaris, G., Kalimeras, E., Iordanidis, F., 2006. Brown tumors of the jaws associated with primary or secondary hyperparathyroidism. A clinical study and review of the literature. American journal of otolaryngology 27, 281–286.

van Baardwijk, A., de Jong, J., Arens, A., Thimister, P., Verseput, G., Kremer, B., Lambin, P., 2006. False-positive FDG-PET scan due to brown tumours. Eur. J. Nucl. Med. Mol. Imaging 33, 393–394.

Zamagni, E.T.P., Cavo, M., 2019. Imaging in multiple myeloma: how? When? Blood 14, 644–651.